JPE 18-4-18

https://doi.org/10.6113/JPE.2018.18.4.1154
ISSN(Print): 1598-2092 / ISSN(Online): 2093-4718

Magnetic-Field-Model and Circuit-Model Based Analysis of Three-Phase Magnetically Coupled Resonant Wireless Power Transfer Systems with Cylinder-Shaped Coils

Xuling Chen†, Xiewei Fu*, Chong Jiang*, Cunhui Pei**, and Fuxin Liu*

*College of Automation Eng., Nanjing University of Aeronautics and Astronautics, Nanjing, China
†,**College of Mechanical and Electrical Eng., Nanjing University of Aeronautics and Astronautics, Nanjing, China

Abstract

In single-phase magnetically coupled resonant (MCR) wireless power transfer (WPT) systems, the transfer characteristics, including the output power and transfer efficiency, are significantly influenced by the spatial scales of its coils. As a potential alternative, a three-phase MCR WPT system with cylinder-shaped coils that are excited in a voltage-fed manner has been proposed to satisfy the requirements of compact space. This system adopts a phase-shifted angle control scheme to generate a rotating magnetic field and to realize omnidirectional WPT that is immune to spatial scales. The magnetic field model and equivalent circuit models are built to holistically analyze the system characteristics under different angular misalignments. Research results show that the transfer characteristics can be improved by modulating the phase-shifted angle in each phase. Experiments have also been carried out to evaluate the accuracy of the theoretical analysis and to confirm the validity of the system modeling method.

Key words: Magnetically coupled resonant, Modelling, three-phase, Wireless power transfer

I. INTRODUCTION

Wireless power transfer (WPT) based on magnetic coupling theory has been increasingly applied in electric vehicles, consumer electronics, implantable medical devices, etc., due to its superiority in terms of being cordless, safe during power charging and able to operate in humid and lousy environments [1]-[7]. Unlike the magnetically coupled inductive (MCI) WPT that adopts a loosely-coupled transformer and only presents high transmission efficiency within centimeters, magnetically coupled resonant (MCR) WPT is a promising technology that uses air-core coils and can be employed in medium-range (10-300cm) applications with a high transmission efficiency [8]. However, among other constraints, the transmission characteristics, which are usually measured by the output power capability and system efficiency, place considerable limits on the range of such applications. Usually, output power and system efficiency are restricted to limited distances and spatial dimensions since the mutual coupling between sending and receiving coils attenuates along with increasing lateral and/or angular misalignments. An urgent issue that needs to be addressed is determining how to realize omnidirectional power transfer for MCR WPT systems to guarantee that the loads can receive power under any misalignment between the sending and receiving coils.

For this purpose, an omni-directional MCR WPT system with two-phase orthogonal coils has been investigated, and it was concluded that an omnidirectional MCR WPT cannot be realized if the two-phase orthogonal coils are driven by identical currents [9]. Furthermore, to extend the power transfer range in spatial scales, three-phase orthogonal coils are adopted in MCR WPT systems, along with a current control method to create a rotating magnetic field, which

Manuscript received Jan. 19, 2018; accepted March 13, 2018
Recommended for publication by Associate Editor Dukju Ahn.
†Corresponding Author: chenxuling@nuaa.edu.cn
Tel: +86-2584892501, Nanjing Univ. of Aeronautics and Astronautics
*College of Automation Eng., Nanjing University of Aeronautics and Astronautics, China
**College of Mechanical and Electrical Eng., Nanjing University of Aeronautics and Astronautics, China

attempts to realize genuine omnidirectional power transfer [9]-[11]. Although multi-phase orthogonal coils are effective for providing continuous power to the load under time-varying misalignments, the magnitude of the current flowing through two- or three-phase sending coils presents much higher than their counterparts in single-phase systems at the same power level. Meanwhile, the two- and three-dimension spherical configurations put forward higher requirements in terms of spatial dimensions. It should be noticed that the systems in the above studies are mostly driven in a current- fed manner, which is not to designe and implemente in practice.

To comprehensively analyze the transmission characteristics of a MCR WPT system, it is necessary to build accurate and effective models to predict the trends of the output power and system efficiency under variable spatial scales. In [12], a mathematical model for a three-phase MCI WPT system was built to enhance the system performance under different horizontal displacements between the sending and receiving coils. Based on the fundamental harmonic analysis (FHA) method, an equivalent circuit model of a single-phase MCR WPT system under varying spatial scales was derived in [13] to analyze the output power and transmission efficiency. However, for three-phase MCR WPT systems, the magnetic field model, which is beneficial to thoroughly comprehend the inherent operation mechanism of systems, as well as confirmation between the magnetic field model and equivalent circuit model, are rarely investigated in existing studies.

Theoretically, both cylinder-shaped and orthogonal circular coils can be adopted in three-phase MCR WPT systems. When compared to orthogonal circular coils, cylinder-shaped coils can achieve a more compact space and a lower current flowing through the sending coils due to the nonzero mutual inductance between any two sending coils. Therefore, in this paper, a three-phase MCR WPT system with cylinder-shaped coils being excited in a voltage-fed manner is discussed in detail. The magnetic field model and the equivalent circuit model of the system adopting phase-shifted angle control are built. Using these models, the transmission characteristics are achieved lucidly and the obtained results are conducive to the modulation of the introduced phase-shifted angle. Finally, a prototype has been built and tested to validate the theoretical analysis.

II. Description of a Three-Phase MCR WPT System with Cylinder-Shaped Coils

Fig. 1 shows a stereogram of the coil configuration in the proposed three-phase MCR WPT system, including the three-phase sending coils and a single-phase receiving coil. All of the sending coils are composed of uniform rectangular coils, where the angle between any two sending coils is 60°. To simplify the analysis, the shape and dimensions of the receiving coil are identical to those of the sending coils and the distance between central axes is d.

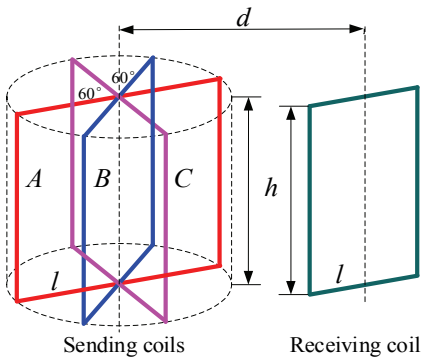

Fig. 1. Stereogram of the cylinder-shaped coils in a three-phase MCR WPT system.

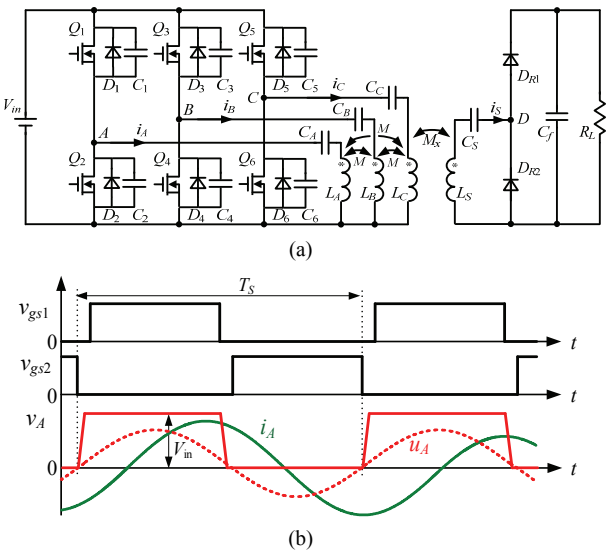

Fig. 2. Driver topology and key waveforms of a three-phase MCR WPT system: (a) Driver topology; (b) Voltage and current waveforms in phase A.

Fig. 2(a) shows the driver topology of a three-phase MCR WPT system, where L_A, L_B, L_C and L_S are the self-inductors of the three sending coils and the receiving coil. C_A, C_B, C_C and C_S are the compensated capacitors in the resonant tank of phase A, B, C and the receiving circuit, respectively. M is the mutual inductance between any two sending coils. M_x (where x represents phase A, B, C) is the mutual inductance between the receiving coil and sending coils. Fig. 2(b) depicts key voltage and current waveforms in phase A as an example, where the dashed line represents the fundamental harmonic of the square-wave voltage v_A.

III. Theoretical Analysis of a Three-Phase MCR WPT System Based on a Magnetic Field Model

In this section, a magnetic field model is built. Then the distribution of the magnetic field strength on the actual trajectory of the receiving coil is calculated using a vector

superstition method, where the variation of the magnetic flux and the induced voltage on the receiving coil can be obtained. On that basis, the output power of the system under different angular misalignments of the receiving coil can be derived directly without the consideration of the mutual coupling between the sending coils and the receiving coil.

A. Magnetic Field Strength Generated by a Current-Carrying Conductor

Fig. 3 shows the magnetic field strength generated by a piece of current-carrying conductor at a random point in space, where line *AB* indicates a piece of electrified wire in space, point *P* is an arbitrary point around the wire, and *Id***l** is the current element in line *AB*. According to the Biot-Savart Law, the magnetic field strength *d***H** on point *P* generated by *Id***l** can be given by:

$$d\mathbf{H} = \frac{I}{4\pi}\frac{d\mathbf{l}\times\mathbf{r}}{r^3} \tag{1}$$

where I is the current flowing through AB, and $\mathbf{r}$ is the distance vector between P and the current element, $\mathbf{r} = (x_0 - x, y_0 - y, z_0 - z)$.

The magnetic field strength **H** generated by the electrified wire AB on point P can be calculated as:

$$\mathbf{H}(x,y,z) = \frac{I}{4\pi}\int\frac{d\mathbf{l}\times\mathbf{r}}{r^3} \tag{2}$$

The derived **H** can be decomposed into three orthogonal components on the x-axis, y-axis and z-axis, and each of the components is expressed as follows:

$$\begin{aligned} H_x &= \frac{I}{4\pi}\left(\int_{y_1}^{y_2}\frac{z_0 - z}{r^3}dy - \int_{z_1}^{z_2}\frac{y_0 - y}{r^3}dz\right) \\ H_y &= \frac{I}{4\pi}\left(\int_{z_1}^{z_2}\frac{x_0 - x}{r^3}dz - \int_{x_1}^{x_2}\frac{z_0 - z}{r^3}dx\right) \\ H_z &= \frac{I}{4\pi}\left(\int_{x_1}^{x_2}\frac{y_0 - y}{r^3}dx - \int_{y_1}^{y_2}\frac{x_0 - x}{r^3}dy\right) \end{aligned} \tag{3}$$

B. Distribution of the Magnetic Field Generated by the Three-Phase Sending Coils

Fig. 4 shows a magnetic field model of a three-phase MCR WPT system in the space rectangular coordinate system, where P_{SA}, P_{SB}, P_{SC} and P_R represent the planes of the sending coils and receiving coil, the x-axis is perpendicular to P_{SA}, and O (the origin of x-axis) is the midpoint of the cylinder-shaped coils. The receiving coil rotates around the z-axis, and circle S is the moving trajectory of P, which is the center point in P_R. d indicates the radius of S. ψ means the included angle between the line PO and the $+x$-axis, which demonstrates the spatial location of the receiving coil.

From Fig. 4, the coordinates of the point in the four sides of P_{SA}, P_{SB}, P_{SC} can be expressed by:

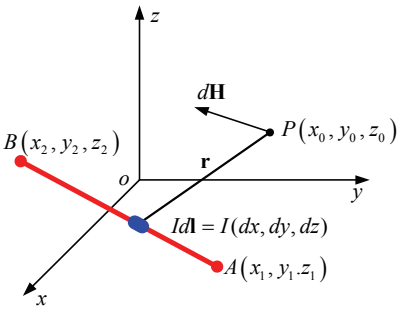

Fig. 3. Current-carrying conductor.

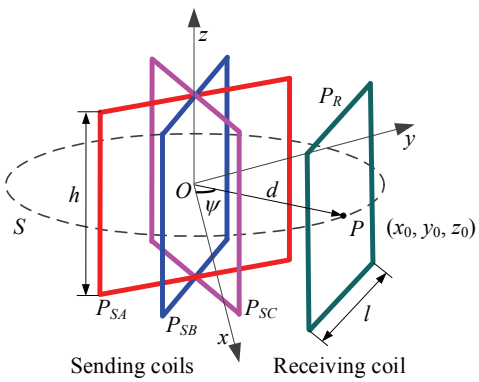

Fig. 4. Magnetic field model of a three-phase MCR WPT system.

$$S:\begin{cases} x = d\cos\psi \\ y = d\sin\psi \\ z = 0 \end{cases},\psi\in[0,2\pi] \tag{4}$$

$$P_{SA}:\begin{cases} x = 0 \\ y = -\dfrac{l}{2} \\ z\in\left[-\dfrac{h}{2},\dfrac{h}{2}\right] \end{cases};\begin{cases} x = 0 \\ y = \dfrac{l}{2} \\ z\in\left[-\dfrac{h}{2},\dfrac{h}{2}\right] \end{cases};\begin{cases} x = 0 \\ y\in\left[-\dfrac{l}{2},\dfrac{l}{2}\right] \\ z = -\dfrac{h}{2} \end{cases};\begin{cases} x = 0 \\ y\in\left[-\dfrac{l}{2},\dfrac{l}{2}\right] \\ z = \dfrac{h}{2} \end{cases} \tag{5}$$

$$P_{SB}:\begin{cases} x = \dfrac{l}{2}\cdot\sin 60^\circ \\ y = -\dfrac{l}{2}\cdot\cos 60^\circ \\ z\in\left[-\dfrac{h}{2},\dfrac{h}{2}\right] \end{cases};\begin{cases} x = -\dfrac{l}{2}\cdot\sin 60^\circ \\ y = \dfrac{l}{2}\cdot\cos 60^\circ \\ z\in\left[-\dfrac{h}{2},\dfrac{h}{2}\right] \end{cases};\begin{cases} x\in\left[-\dfrac{l}{2}\cdot\sin 60^\circ,\dfrac{l}{2}\cdot\sin 60^\circ\right] \\ y = -x\cdot\tan 30^\circ \\ z = -\dfrac{h}{2} \end{cases};\begin{cases} x\in\left[-\dfrac{l}{2}\cdot\sin 60^\circ,\dfrac{l}{2}\cdot\sin 60^\circ\right] \\ y = -x\cdot\tan 30^\circ \\ z = \dfrac{h}{2} \end{cases} \tag{6}$$

$$P_{SC}:\begin{cases}x=\dfrac{l}{2}\cdot\sin 60°\\ y=\dfrac{l}{2}\cdot\cos 60°;\\ z\in\left[-\dfrac{h}{2},\dfrac{h}{2}\right]\end{cases}\begin{cases}x=-\dfrac{l}{2}\cdot\sin 60°\\ y=-\dfrac{l}{2}\cdot\cos 60°;\\ z\in\left[-\dfrac{h}{2},\dfrac{h}{2}\right]\end{cases}\tag{7}$$

$$\begin{cases}x\in\left[-\dfrac{l}{2}\cdot\sin 60°,\dfrac{l}{2}\cdot\sin 60°\right]\\ y=x\cdot\tan 30°\\ z=-\dfrac{h}{2}\end{cases};\begin{cases}x\in\left[-\dfrac{l}{2}\cdot\sin 60°,\dfrac{l}{2}\cdot\sin 60°\right]\\ y=x\cdot\tan 30°\\ z=\dfrac{h}{2}\end{cases}$$

To generate a rotating magnetic field, a phase-shifted angle control scheme is adopted in this paper [12]. Since the magnetic field strength is directly dependent on the exciting currents, the currents flowing through the three-phase sending coils are pre-designed and given by:

$$\begin{aligned}i_A&=I_m\sin(\omega t)\\ i_B&=I_m\sin(\omega t+\varphi)\\ i_C&=I_m\sin(\omega t+2\varphi)\end{aligned}\tag{8}$$

where I_m is the magnitude of the currents that can be derived according to the specific phase voltage, ω is the angular frequency, and φ is the introduced phase-shifted angle.

The resultant magnetic fields $\mathbf{H}=(H_x, H_y, H_z)$ generated by the three-phase currents can be calculated based on the superposition principle of the magnetic field.

$$\begin{aligned}H_x&=N_S\times(H_{xA}+H_{xB}+H_{xC})\\ H_y&=N_S\times(H_{yA}+H_{yB}+H_{yC})\\ H_z&=N_S\times(H_{zA}+H_{zB}+H_{zC})\end{aligned}\tag{9}$$

where N_S is the turns number of the sending coils, and the components on each of the axes can be obtained by substituting the coordinates of the points in the four sides of P_{SA}, P_{SB}, P_{SC} and the circle S into (3). From (9), Fig. 5 shows the magnetic field magnitude on the circle S generated by the sending coils with phase-shifted angles of 0° and 60° at different times, where H is the amplitude of the vector $\mathbf{H}$, $H=(H_x^2+H_y^2+H_z^2)^{1/2}$ The parameters are listed in Table. I.

Fig. 6 shows the curves of the magnetic field magnitude as a function of ψ at four specific times, which is partially intercepted from Fig. 5. As depicted in Fig. 6(a), when φ=0°, i.e., the three-phase currents flowing through the sending coils are identical, the variation tendencies of the magnetic field strength at different times on the circle S are similar. Nevertheless, the magnitudes of all the curves differ from each other due to the different amplitudes of the exciting ac currents. This demonstrates that the resultant vector direction of the magnetic field is always constant, and that the maximum magnetic field strength occurs at the points ψ=0° and ψ=180°. Meanwhile, the minimum magnetic field

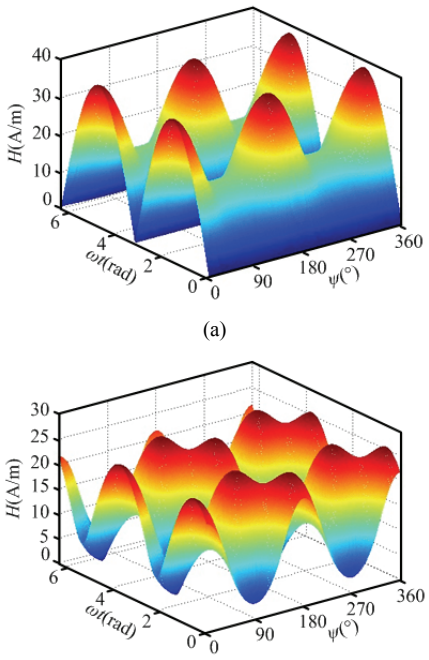

Fig. 5. Three-dimensional diagram of the magnetic field magnitude: (a) φ=0°; (b) φ=60°.

TABLE I
PARAMETERS OF THE MAGNETIC FIELD MODEL

Parameter	Value	Parameter	Value
l	0.22m	I_m	24A
h	0.3m	N_S	1
d	0.25m	ω	$2\pi\times100\times10^3$rad

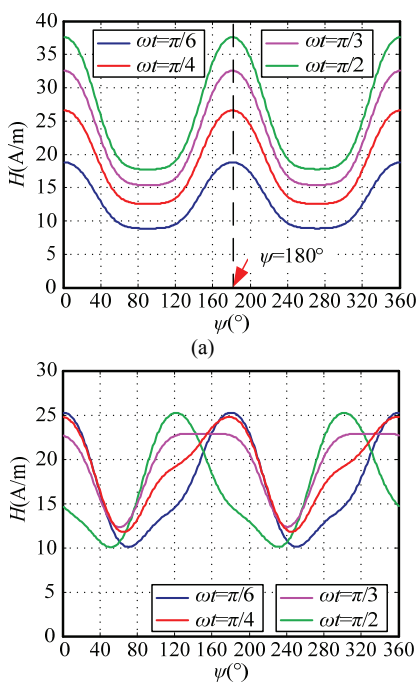

Fig. 6. Magnitude of the magnetic field strength at different times: (a) φ=0°; (b) φ=60°.

strength always appears at ψ=90° and ψ=270°, which shows that the generated magnetic field is weak and barely builds the energy transmission channel between the sending and receiving coils. It also shows that the dead zone for the power transfer inherently exists on the circle *S*. In Fig. 6(b), when the phase-shifted angle is introduced into the exciting ac currents, the maximum value of *H* at different times shifts along with ψ rather than being fixed at some specific ψ, which means that the direction of the resultant magnetic field vector rotates around the central axis of the sending coils and achieves omnidirectional power transfer.

C. Induced Voltage on the Receiving Coil and Output Power

The magnetic flux ϕ in the receiving coil can be obtained as:

$$\phi = \mu_0 \cdot N_S \iint \mathbf{H} d\mathbf{P_R} = \mu_0 \iint \left(H_x, H_y, H_z\right) \mathbf{n} d\mathbf{P_R} \tag{10}$$

where μ_0 is the magnetic permeability of the free-space, $\mathbf{P_R}$ represents the plane of the receiving coil, and **n** represents the unit normal vector of the receiving coil plane, **n**=(cosψ, sinψ, 0).

From (10), the induced voltage on the receiving coil can be derived according to the Faraday law of electromagnetic induction. Then the transmission power can be further calculated by:

$$P_o = \left(\frac{u_R}{r_S + R_W}\right)^2 \cdot R_W \tag{11}$$

where, u_R and r_S are the induced voltage and parasitic resistance of the receiving coil, respectively. R_W is the equivalent impedance of the circuit from the point of view of the voltage-double rectifier, which will be given in Section IV. In addition, the theoretical results based on the magnetic field model will be illustrated in Section V.

It should be noted that the transmission efficiency is difficult to determine despite the obtained output power since the input power cannot be derived directly by a magnetic field model.

D. Simulation of the Magnetic Field Model by Maxwell

To verify the derivation of the magnetic field strength generated by three-phase exciting currents, a finite element simulation by Maxwell is carried out to achieve the magnetic field strength without complicated mathematical calculations. An electromagnetic simulation model of cylinder-shaped sending coils in Maxwell is given in Fig. 7, and the parameters of the system are the same as those in Table I.

Taking two typical cases as examples, the distributions of the magnetic field on the circle S are intuitively shown in Fig. 8, where the magnitude variations of the magnetic field are represented by different colors (red means maximum and blue means minimum). Fig. 9 shows the curves of H as a function of ψ, which is derived from Fig. 8, where the solid

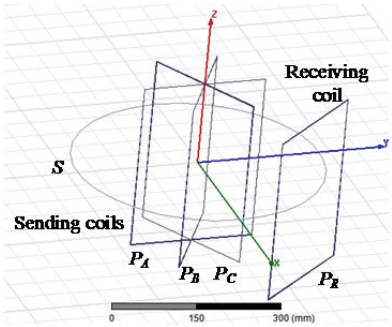

Fig. 7. Simulation model of a three-phase MCR WPT system in Maxwell

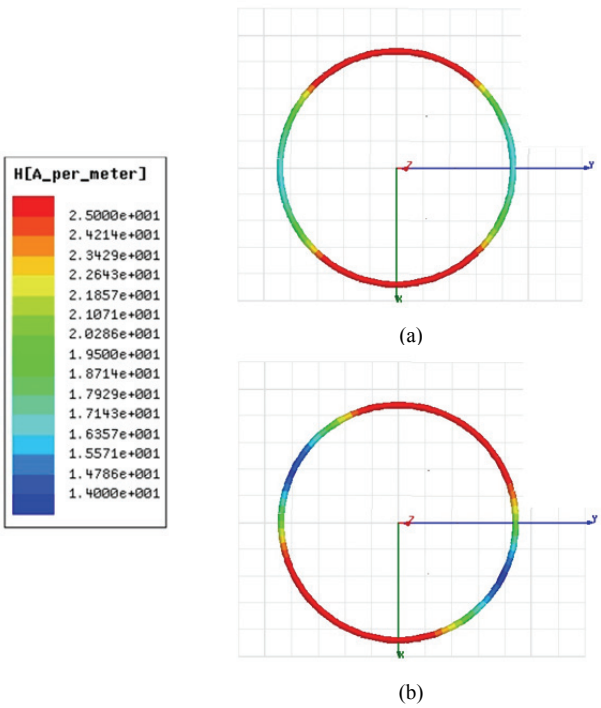

(a)

(b)

Fig. 8. Distribution of the magnetic field on the circle S around the cylinder-shaped sending coils: (a) φ=0°, ωt=π/3; (b) φ=60°, ωt=π/3.

line is the simulation data and the dashed line is the calculated data based on the magnetic field model. It is observed that the calculated results are consistently accordant with the simulation results, which indicates that the magnetic field model is effective, and that the theoretical calculation is accurate for demonstrating the magnetic field distribution.

IV. Theoretical Analysis of the Three-Phase MCR WPT System Based on a Circuit Model

In this section, the FHA method is implemented to derive an equivalent circuit model of the three-phase MCR WPT system in the steady state. Meanwhile, the mutual inductances between the sending coils and the receiving coil under varying angular misalignments are calculated by mathematical

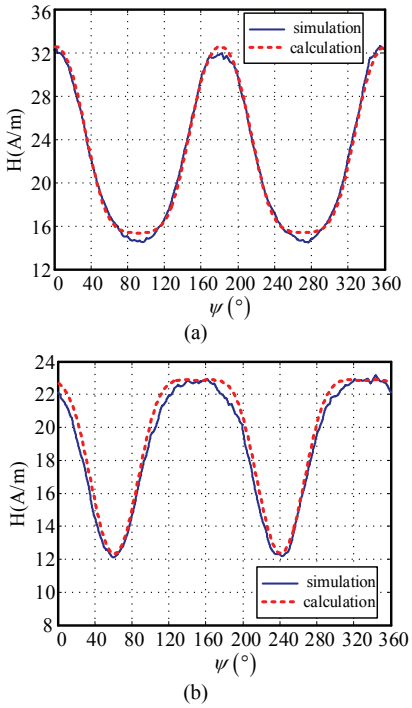

Fig. 9. Comparisons between the simulation data and calculated data: (a) φ=0°, ωt=π/3; (b) φ=60°, ωt=π/3.

methods, which serve as the intermediate variable to deduce the transmission characteristics. In order to simplify the analysis, the following assumptions are made:

1) The resonant inductors are L_A=L_B=L_C=L_S=L, and the resonant capacitors are C_A=C_B=C_C=C_S=C;

2) The parasitic resistances of the coils are R_P=R_S, and they are assumed to be constant.

A. Equivalent Circuit Model Using the Fundamental Harmonic Analysis Method

Fig. 10 shows a decoupled equivalent circuit of the system derived by the FHA method, where the mutual inductances between the sending coils and the receiving coil are equivalent to current-controlled voltage sources. The three-phase equivalent voltage sources are expressed by (12) with an introduced phase-shifted angle φ.

$$\begin{aligned} u_A(t) &= U_m \cos(\omega t) \\ u_B(t) &= U_m \cos(\omega t + \varphi) \\ u_C(t) &= U_m \cos(\omega t + 2\varphi) \end{aligned} \tag{12}$$

where U_m is the maximum value of the equivalent exciting voltage.

Due to the half-bridge configuration, the norm of $\dot{U}_S$ can be calculated as:

$$U_S = \left\|\dot{U}_S\right\| = \frac{\sqrt{2}}{\pi} V_{in} \tag{13}$$

The relationship between the equivalent load resistance R_W and the real load resistance R_L is:

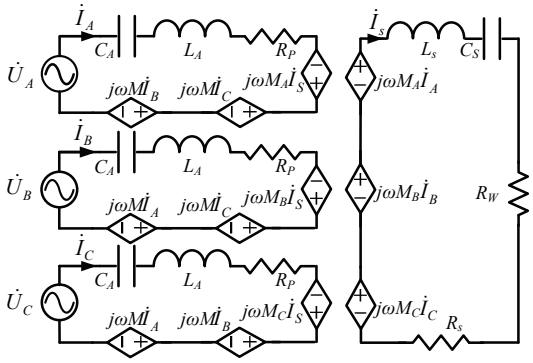

Fig. 10. Decoupled equivalent circuit model of the three-phase MCR WPT system.

$$R_W = \frac{2}{\pi^2} R_L \tag{14}$$

From Fig. 10, the following equation can be obtained by Kirchhoff's voltage law:

$$\begin{bmatrix} \dot{U}_A \\ \dot{U}_B \\ \dot{U}_C \end{bmatrix} = \begin{bmatrix} Z_p & j\omega M & j\omega M \\ j\omega M & Z_p & j\omega M \\ j\omega M & j\omega M & Z_p \end{bmatrix} \begin{bmatrix} \dot{I}_A \\ \dot{I}_B \\ \dot{I}_C \end{bmatrix} - \begin{bmatrix} j\omega M_A \\ j\omega M_B \\ j\omega M_C \end{bmatrix} \left[\dot{I}_S\right] \tag{15}$$

$$[0] = \begin{bmatrix} j\omega M_A & j\omega M_B & j\omega M_C \end{bmatrix} \begin{bmatrix} \dot{I}_A \\ \dot{I}_B \\ \dot{I}_C \end{bmatrix} - [Z_S]\left[\dot{I}_S\right] \tag{16}$$

Since the resonant frequencies of both the sending and receiving coils are equal to the switching frequency:

$$Z_P = R_P + j\omega L + \frac{1}{j\omega C} = R_P \tag{17}$$

$$Z_S = \left(R_S + R_W\right) + j\omega L + \frac{1}{j\omega C} = R_S + R_W \tag{18}$$

Assuming that:

$$\mathbf{U} = \begin{bmatrix} \dot{U}_A & \dot{U}_B & \dot{U}_C \end{bmatrix}^T \tag{19}$$

$$\mathbf{I} = \begin{bmatrix} \dot{I}_A & \dot{I}_B & \dot{I}_C \end{bmatrix}^T \tag{20}$$

$$\mathbf{A} = \begin{bmatrix} Z_P & j\omega M & j\omega M \\ j\omega M & Z_P & j\omega M \\ j\omega M & j\omega M & Z_P \end{bmatrix} \tag{21}$$

$$\mathbf{B} = \begin{bmatrix} j\omega M_A & j\omega M_B & j\omega M_C \end{bmatrix} \tag{22}$$

Substituting (19)-(22) into (15) and (16) yields:

$$\mathbf{U} = \mathbf{A} \cdot \mathbf{I} - \mathbf{B}^{\mathbf{T}} \cdot \dot{I}_S \tag{23}$$

$$[0] = \mathbf{B} \cdot \mathbf{I} - Z_s \cdot \dot{I}_S \tag{24}$$

Therefore, the input current $\mathbf{I}$, the output current $\dot{I}_S$, the output power P_{out}, and the transmission efficiency η can be expressed by:

$$\mathbf{I} = Z_s \left(Z_s \mathbf{A} - \mathbf{B}^T \mathbf{B}\right)^{-1} \mathbf{U} \tag{25}$$

$$\dot{I}_S = \mathbf{B}\left(Z_S\mathbf{A} - \mathbf{B}^T\mathbf{B}\right)^{-1}\mathbf{U} \tag{26}$$

$$P_{out} = \mathrm{Re}\left(R_W \dot{I}_S \dot{I}_S^*\right) \tag{27}$$

$$P_{in} = \mathrm{Re}(\dot{U}_A\dot{I}_A{}^* + \dot{U}_B\dot{I}_B{}^* + \dot{U}_C\dot{I}_C{}^*) \tag{28}$$

$$\eta = P_{out} / P_{in} \tag{29}$$

Equations (27) and (29) show that P_{out} and η are affected by the phase-shifted angle, which determines the distribution of the magnetic field around the sending coils. Furthermore, the positions and turns of the coils that directly impact the mutual inductance also have influences on P_{out} and the other system performances.

B. Mutual Inductance under Varying Angular Misalignments

From the above mentioned analysis, it is clearly indicated that the transmission characteristics are highly relevant to the mutual inductances that are further strongly influenced by the varying rotating angular misalignments of the receiving coil. Fig. 11 illustrates a planform of the coils under different values of ψ, where the variation range of ψ is 0° ~ 180° due to the symmetric distribution of the magnetic field according to the aforementioned analysis on magnetic field model.

To describe the relationship between the transmission characteristics and the angular misalignment, the mutual inductance model of two arbitrary rectangular coils in space is built in Fig. 12, where the four sides of the two rectangular coils are respectively represented by a_1, b_1, c_1, d_1 and a_2, b_2, c_2, d_2. S and R are two random points on the coils, and the distance between S and R is r_{SR}. Point P is the center of the upper coil, H is the vertical displacement on the z-axis, and L is the lateral displacement on the x-axis. **n** is the normal vector of the upper coil, and the included angle between **n** and the +x-axis is ψ.

The mutual inductance of any two lines can be obtained by solving the Neumann's formula:

$$M = \frac{\mu_0 N_S N_R}{4\pi}\oint\oint \frac{\mathbf{dl_S}\cdot\mathbf{dl_R}}{r_{SR}} \tag{30}$$

where N_S, N_R, $\mathbf{l_S}$, $\mathbf{l_R}$, $\mathbf{dl_S}$ and $\mathbf{dl_R}$ are the turns, the length vector of each turn and the infinitesimal of the coils, respectively.

From Fig. 12, the coordinates of S, R, $\mathbf{dl_P}$, and $\mathbf{dl_S}$ on four sides of the two rectangular coils are given in Table II.

Substituting the coordinates of S, R, $\mathbf{dl_P}$, and $\mathbf{dl_S}$ on the four sides of the two rectangular coils into (30), the mutual inductance between any two sides of the rectangular coils can be calculated. Further, the mutual inductance between the two rectangular coils can be achieved by the superposition method, i.e.:

$$\begin{aligned} M_{total} = {} & M_{a_1a_2} + M_{a_1c_2} + M_{b_1b_2} \\ & + M_{b_1d_2} + M_{c_1c_2} + M_{c_1a_2} + M_{d_1d_2} + M_{d_1b_2} \end{aligned} \tag{31}$$

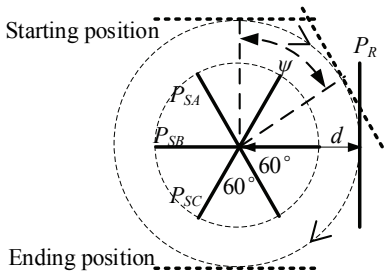

Fig. 11. Planform of the coils.

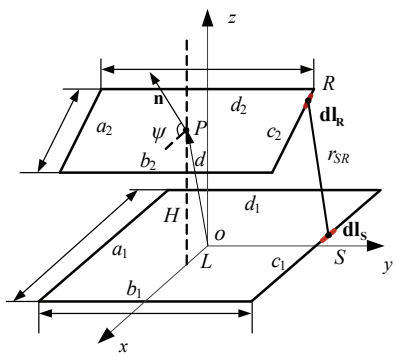

Fig. 12. Mutual inductance model.

TABLE II
COORDINATES OF TWO RANDOM POINTS ON RECTANGULAR COILS

$S(x_1,y_1,z_1)$	$\mathbf{dl_S}$	$R(x_2,y_2,z_2)$	$\mathbf{dl_R}$
$\left(x_1,-\frac{b_1}{2},0\right)$, $x_1\in\left[-\frac{a_1}{2},\frac{a_1}{2}\right]$	$(dx_1,0,0)$	$\left(x_2,-\frac{b_2}{2},-x_2\tan^{-1}\psi+H\right)$, $y_2\in\left[-\frac{a_2}{2}\sin\psi,\frac{a_2}{2}\sin\psi\right]$	$(dx_2,0,dz_2)$
$\left(\frac{a_1}{2},y_1,0\right)$, $y_1\in\left[-\frac{b_1}{2},\frac{b_1}{2}\right]$	$(0,dy_1,0)$	$\left(\frac{a_2}{2}\sin\psi,y_2,H-\frac{a_2}{2}\cos\psi\right)$, $y_2\in\left[-\frac{b_2}{2},\frac{b_2}{2}\right]$	$(0,dy_2,0)$
$\left(x_1,\frac{b_1}{2},0\right)$, $x_1\in\left[-\frac{a_1}{2},\frac{a_1}{2}\right]$	$(dx_1,0,0)$	$\left(x_2,\frac{b_2}{2},-x_2\tan^{-1}\psi+H\right)$, $x_2\in\left[-\frac{a_2}{2}\sin\psi,\frac{a_2}{2}\sin\psi\right]$	$(dx_2,0,dz_2)$
$\left(-\frac{a_1}{2},y_1,0\right)$, $y_1\in\left[-\frac{b_1}{2},\frac{b_1}{2}\right]$	$(0,dy_1,0)$	$\left(-\frac{a_2}{2}\sin\psi,y_2,H+\frac{a_2}{2}\cos\psi\right)$, $y_2\in\left[-\frac{b_2}{2},\frac{b_2}{2}\right]$	$(0,dy_2,0)$

Considering the fixed positions of the three-phase sending coils, the mutual inductance M between the sending coils are constants determined to be $21.1\times10^{-6}\mu$H from (31). The specifications are listed as follows: N_P=N_S=14, a_1=a_2=0.22m, b_1=b_2=0.3m and d=0.25m. Fig. 13 shows the curves of the mutual inductance M_x (x=A, B, C) between the receiving coil and the sending coils according to (31). It can be known that M_A, M_B and M_C vary along with the angular misalignment in an interleaved manner. In addition, the interleaved angular difference is 60°.

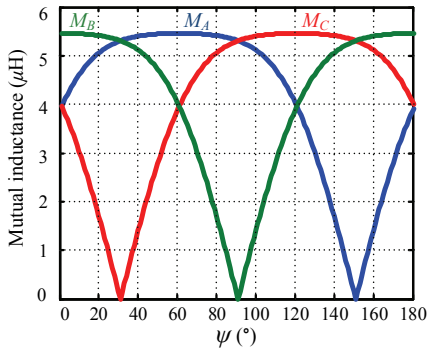

Fig. 13. Mutual inductances between the receiving coil and the sending coils.

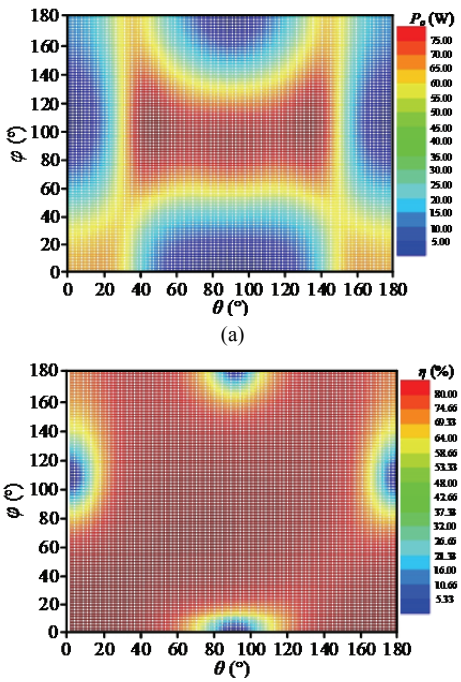

Fig. 14. Transmission characteristics under different phase-shifted angles and angular misalignments: (a) Output power; (b) Transmission efficiency.

C. Output Power and Transmission Efficiency

The output power and the transmission efficiency can be calculated by substituting the achieved mutual inductances into (27) and (29). Fig. 14 depicts color maps of the transmission characteristics with different phase-shifted angles and angular misalignments, where the output power or transmission efficiency decreases from its maximum to its minimum along with the color changing from red to blue. The parameters of the illustrative case are listed as follows: f_s=100 kHz, V_{in}=72V, R_S= R_P =0.23Ω and R_L=5Ω. As shown in Fig. 14, the output power or transmission efficiency is maintained at a relatively stable level when a proper phase-shifted angle is adopted. For example, in Fig. 14(a), when φ is designed within [60°-130°], the output power is nearly constant as ψ varies from 40° to 140°. In Fig. 14(b), when φ is designed within [20°- 80°] or [140°-160°], the transmission efficiency is keep nearly constant under any angular misalignment, which indicates that the design of the phase-shifted angle can be optimized to achieve a steady transmission characteristics within a specific variation of the angular misalignment. It is also determined that the phase-shifted angle has an impact on the soft-switching conditions of the power switches in the driver inverter. Therefore, the specific phase-shifted angle should be designed based on the optimal results of both the output power and the switching conditions of the switches, which will be investigated in a future work.

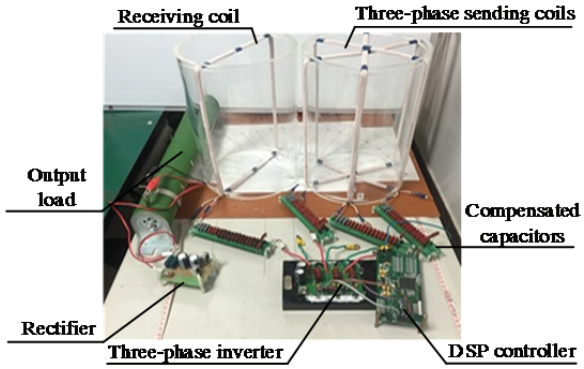

Fig. 15. Prototype of the cylinder-shaped three-phase MCR WPT system.

TABLE III
PARAMETERS OF THE PROTOTYPE

Parameter		Symbol	Value
Transmitter	Turns	N_P	14
	resistance	R_P	0.23Ω
	self-inductors	L_x	L_A=142.12μH, L_B=143.02μH, L_C=145.82μH
	compensated capacitors	C_x	C_A=17.82nF, C_B=17.71nF, C_C=17.37nF
Receiver	Turns	N_S	14
	resistance	R_S	0.23Ω
	self-inductors	L_S	L_S=142.67μH
	compensated capacitors	C_S	C_S=17.8nF
Input voltage		V_{in}	72V
Load		R_L	5Ω
Operating frequency		f_s	100kHz
Transmission distance		d	25cm

V. EXPERIMENTAL VERIFICATIONS

In order to validate the theoretical analysis, a prototype has been built and tested in the laboratory, as shown in Fig. 15. The main specifications and coil parameters are listed in Table III.

Figs. 16-17 illustrate experimental and theoretical curves of the transmission characteristics with full angular

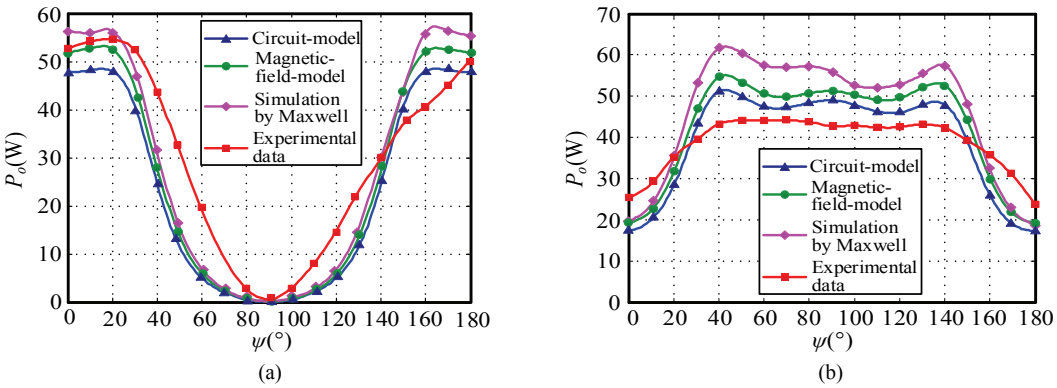

Fig. 16. Output power with full angular misalignment under different phase-shifted angles: (a) φ=0°; (b) φ=60°.

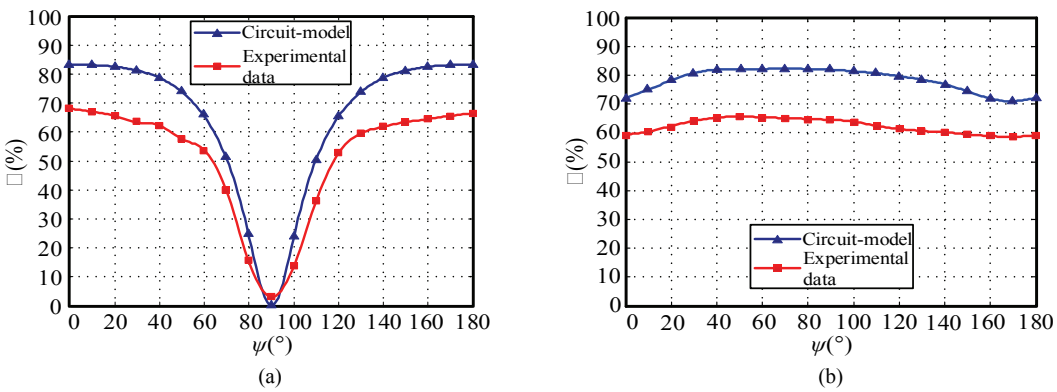

Fig. 17. Transmission efficiency with full angular misalignment under different phase-shifted angles: (a) φ=0°; (b) φ=60°.

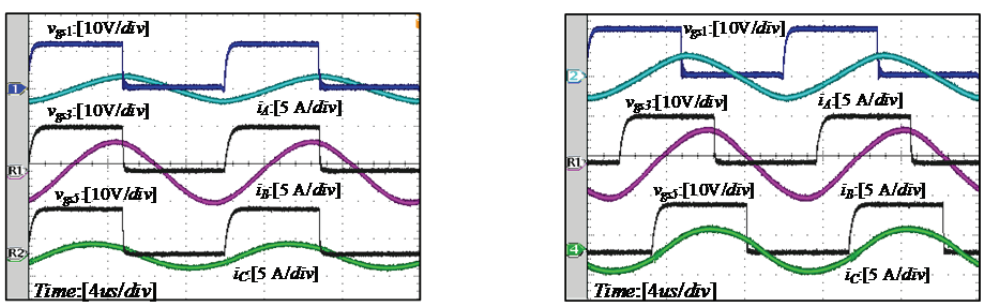

Fig. 18. Experimental waveforms under different angular misalignments and phase-shifted angles: (a) φ=0°, ψ=30°; (b) φ=60°, ψ=150°.

misalignment when the phase-shifted angle is adopted as φ=0º and φ=60º, where the given three-phase currents in the magnetic field model are determined by experimental data. From Figs. 16-17, it is observed that the trends of the experimental results consistently match those of the theoretical data based on the circuit model and magnetic field model. The error between the calculated and measured data is relatively minor, which proves that the modeling method applied on the three-phase MCR WPT system is effective and able to accurately describe the transmission characteristics. Since the transmission efficiency is difficult to be calculated by the magnetic field model, only experimental data and theoretical data based on a circuit model are given in Fig. 17. As can be seen, when φ=0°, the output power and transmission efficiency decrease dramatically to their minimums as ψ approaches 90°, and a dead zone for power transfer appears at around ψ=90°. However, when φ=60°, the transmission power and efficiency are nearly stable within a wide range of angular misalignments, which shows that the modulation of the phase-shifted angle is an effective method to realize omnidirectional MCR WPT.

Fig. 18 shows experimental waveforms under various angular misalignments and different phase-shifted angles. As can be seen, the waveforms of the currents flowing through three-phase sending coils are nearly standard sinusoidal waveforms, which demonstrates that FHA method can be

employed to analyze the transmission characteristics in an equivalent circuit model.

VI. CONCLUSIONS

This paper investigated two intensive analytical models for a three-phase MCR WPT system with cylinder-shaped coils, i.e., a magnetic field model and an equivalent circuit model. The magnetic field model can directly illustrate the distribution of the magnetic field around the sending coils, where the induced voltage of the receiving coil and the output power of the system can be calculated with the given three-phase input currents. However, the transmission efficiency is barely derived by the magnetic field model. When compared with the magnetic field model, the equivalent circuit model can describe the transmission characteristics more clearly by adopting the FHA method and the given mutual inductance between coils, which is more effective and intuitive for theoretical analysis and parameters design. The derived results from both analytical models are in good agreement with each other. They are also shown to be valid by the experimental data. In a future work, the optimization of the phase-shifted angle and a theoretical analysis of the system with a small-scale receiving coil will be implemented to achieve stable transmission characteristics and to satisfy the requirements of practical applications.

ACKNOWLEDGMENT

This work was financially supported by the National Natural Science Foundation of China (51505223), the Fundamental Research Funds for the Central Universities of China (NS2015047), the Natural Science Foundation of Jiangsu Province, China (BK20151471), and the Lite-on Research Program.

REFERENCES

[1] S. Y. R. Hui, W. X. Zhong, and C. K. Lee, "A critical review on recent progress in mid-range wireless power transfer," *IEEE Trans. Power Electron.*, Vol. 29, No. 9, pp. 4500-4511, Sep. 2014.

[2] N. Shinohara, "Wireless power transmission progress for electric vehicle in Japan," *Proc. IEEE Radio and Wireless Symposium*, pp. 109-111, 2013.

[3] G. A. Covic and J. T. Boys, "Inductive power transfer," *Proc. IEEE*, Vol. 101, No. 6, pp. 1276-1289, Jun. 2013.

[4] S. Y. R. Hui and W. W. C. Ho, "A new generation of universal contactless battery charging platform for portable consumer electronic equipment," *IEEE Trans. Power Electron.*, Vol. 20, No. 3, pp. 620-627, May 2005.

[5] S. Y. Hui, "Planar wireless charging technology for portable electronic products and Qi," *Proc. IEEE*, Vol. 101, No. 6, pp. 1290-1301, Jun. 2013.

[6] H. G. Lim, Y. H. Yoon, C.W. Lee, I. Y. Park, B. S. Song, and J. H. Cho, "Implementation of a transcutaneous charger for fully implantable middle ear hearing device," in *Proc. IEEE Conference of Engineering in Medicine and Biology Society*, pp. 6813-6816, 2005.

[7] C. K. Lee, W. X. Zhong, and S. Y. R. Hui, "Recent progress in mid-range wireless power transfer," in *Proc. IEEE Energy Conversion Congress and Exposition*, pp. 3819-3824, 2012.

[8] A. Kurs, A. Karalis, R. Moffatt, J. D. Joannopoulos, P. Fisher, and M. Soljacic, "Wireless power transfer via strongly coupled magnetic resonances," *Science*, Vol. 317, No. 5834, pp. 83-86, Jul. 2007.

[9] W. M. Ng, C. Zhang, D Lin, and S. Y. R. Hui, "Two- and Three- Dimensional Omni-Directional Wireless Power Transfer," *IEEE Trans. Power Electron.*, Vol. 29, No. 9, pp. 4470-4474, Jan. 2014.

[10] D. Wang, Y. Zhu, Z. Zhu, T. T. Mo, and Q. Huang, "Enabling multi-angle wireless power transmission via magnetic resonant coupling," in *Proc. 7th International Conference on Computing and Convergence Technology (ICCCT)*, pp. 1395-1400, 2012.

[11] C. Zhang, D. Lin, and S. Y. R. Hui, "Basic control principle of 3-dimensional omnidirectional wireless power transfer," *IEEE Trans. Power Electron.*, Vol. 31, No. 7, pp. 5215-5227, Jul. 2016.

[12] H. Matsumoto, Y. Neba, K. Ishizaka, and R. Itoh, "Model for a three-phase contactless power transfer system," *IEEE Trans. Power Electron.*, Vol. 26, No. 9, pp. 2676-2687, Sep. 2011.

[13] F. X. Liu, Y. Yang, D. Jiang, X. B. Ruan, and X. L. Chen, "Modeling and optimization of magnetically coupled resonant wireless power transfer system with varying spatial scales", *IEEE Trans. Power Electron.*, Vol. 32, No. 4, pp. 3240-3250, Sep. 2017.

Xuling Chen was born in Hunan Province, China, in 1979. She received her B.S., M.S. and Ph.D. degrees in Mechanical and Electrical Engineering from the Nanjing University of Aeronautics and Astronautics (NUAA), Nanjing, China, in 2002, 2005 and 2011, respectively. In 2005, she joined the Faculty of the College of Automation Engineering, NUAA, where she is presently working as a Lecturer. In 2017, she joined the Department of Electrical and Computer Engineering, Technical University of Munich, Munich, Germany, where she served as a Visiting Scientist. Her current research interests include wireless power transfer, mechanical and electrical engineering, and mechanical design.

Xiewei Fu was born in Hubei Province, China. He received his B.S. degree in Electrical Engineering and Automation from the Nanjing University of Aeronautics and Astronautics (NUAA), Nanjing, China, in 2015, where he is presently working towards his M.S. degree in Electrical Engineering. His current research interests include wireless power transfer.

Chong Jiang was born in Jiangsu Province, China. She received her B.S. and M.S. degrees in Electrical Engineering and Automation from the Nanjing University of Aeronautics and Astronautics (NUAA), Nanjing, China, in 2014 and 2017, respectively. Her current research interests include wireless power transfer.

Cunhui Pei was born in Jiangsu Province, China, in 1991. He received his B.S. degree from the Department of Mechanical and Electrical Engineering, Jiangsu University of Science and Technology (JUST), Jiangsu, China, in 2016. He is presently working towards his M.S. degree at the Nanjing University of Aeronautics and Astronautics (NUAA), Nanjing, China. His current research interests include wireless power transfer and mechanical design.

Fuxin Liu was born in Heilongjiang Province, China, in 1979. He received his B.S., M.S. and Ph.D. degrees in Electrical Engineering from the Nanjing University of Aeronautics and Astronautics (NUAA), Nanjing, China, in 2001, 2004 and 2007, respectively. In 2007, he joined the Faculty of the College of Automation Engineering, NUAA, where he is presently working as an Associate Professor. In 2017, he joined the Department of Electrical and Computer Engineering, Technical University of Munich (TUM), Munich, Germany, where he served as a Visiting Professor. His current research interests include wireless power transfer, soft-switching dc/dc converters, and renewable energy generation systems. Dr. Liu was awarded the August-Wilhelm Scheer Visiting Professorship of TUM, and he is serving as an Honorary Fellow of the TUM Institute for Advanced Study.